American Mineralogist, Volume 79, pages 838–847, 1994

Structural environment of Zr in two inosilicates from Cameroon: Mineralogical and geochemical implications

François Farges*
Laboratoire de Physique et Mécanique des Géomatériaux, Université Marne la Vallée (IPGP and UA CNRS 734), 2 allée de la Butte Verte, 93160 Noisy le Grand, France

Gordon E. Brown, Jr.
Department of Geological and Environmental Sciences and Stanford Synchrotron Radiation Laboratory, Stanford University, Stanford, California 94305-2115, U.S.A.

Danielle Velde
Laboratoire de Pétrologie Minéralogique, Université Paris 6, 4 place Jussieu, 75252 Paris Cedex 05, France

Abstract

The structural environments of Zr in a Na- and Fe^{2+}-rich clinopyroxene and an arfvedsonitic amphibole (both with 1–2 wt% ZrO_2) from a phonolite of the Rumpi Hills volcanic complex, west Cameroon, were examined using X-ray absorption fine-structure (XAFS) spectroscopy at the Zr*K* edge. In the clinopyroxene, tetravalent Zr is coordinated by six O atoms. Mean d[Zr-O] ≈ 2.07(1) Å; second neighbors around Zr include (Si,Na) and Fe at ≈3.16–3.18(5) Å. No evidence was found for Zr second neighbors. These observations are consistent with the presence of Zr in the M1 site. This structural arrangement leads to local bond valence satisfaction and supports the mechanism for Zr substitution in inosilicates suggested by Jones and Peckett (1980). Similarities in the XANES and XAFS spectra of clinopyroxene and arfvedsonite suggest that Zr is located in the M2 site in arfvedsonite, with mean d[Zr-O] ≈ 2.04(4) Å.

The local environment of Zr in these Na- and Fe^{2+}-rich inosilicates is like that observed in Zr-bearing garnets and Zr-bearing silicate glasses, in which $^{[6]}$Zr is favored by the presence of nonbridging O atoms, to which Zr preferentially bonds. The similarity of the short-range structural environment of Zr in silicate melts and in $^{[6]}$Zr-, Na-, and Fe^{2+}-bearing inosilicates may explain why this normally incompatible trace element behaved compatibly during the crystallization of the phonolites of the Rumpi Hills volcanic complex, in which Na- and Fe^{2+}-rich inosilicates are found. Simple bond valence arguments are used to explain why increases in the Fe^{3+}-Fe_{tot} ratio during later stages of differentiation of the Rumpi Hills peralkaline melt should favor the incompatible behavior of Zr.

Introduction

Zr is a tetravalent trace element (Dunn and McCallum, 1982) often used as an indicator of magmatic processes (Allègre et al., 1977; Hildreth, 1979; Pearce and Norry, 1979; Henderson, 1982; Hofmann, 1988), mainly because of its incompatible character (Treuil et al., 1979), particularly in peralkaline rock suites (Dunn and McCallum, 1982) in which Zr solubility is high (Watson, 1979; Watson and Harrison, 1983). Mineral-liquid partition coefficients for Zr ($D^{Zr}_{mineral\text{-}liquid}$) (e.g., Lemarchand et al., 1987) are low for most minerals (typically $D^{Zr} < 0.1$); however, significantly higher D^{Zr} values have been reported for some titanium oxides, garnets, and inosilicates ($D^{Zr} \approx 0.1$–0.8: McCallum and Charette, 1978; Larsen, 1979; Dunn and McCallum, 1982; Fujimaki et al., 1984; Watson and Ryerson, 1986; Green et al., 1989; and others). For example, electron microprobe analyses have shown that ZrO_2 concentrations up to 8 wt% are not uncommon in small zones of Na- and Fe-rich clinopyroxene, amphibole, and aenigmatite grains from volcanic rocks (trachytes and phonolites) from Mururoa, French Polynesia (Wagner et al., 1988), central New South Wales (Duggan, 1988), and the Rumpi Hills, Cameroon (Nkoumbou, 1990), and in alkaline igneous rocks (nepheline syenites and peralkaline granites) from Greenland (Jones and Peckett, 1980; Pearce, 1989, 1990); however, these minerals may be compositionally zoned, and the average ZrO_2 content is often considerably lower.

The reason why Zr readily partitions from alkali silicate magmas into Na-rich inosilicates is poorly understood, primarily because of a lack of direct information on the kind of structural sites occupied by trace to minor Zr in these phases. The present study utilized X-ray absorption fine-structure (XAFS) spectroscopy to examine

* Present address: Laboratoire des Géomatériaux, IPGP, 4 place Jussieu, 75005 Paris, France.

0003–004X/94/0910–0838$02.00

TABLE 1. Bulk rock, CIPW norms, and modal analysis of the phonolite NK 30

Bulk rock analysis (wt%)		CIPW norm		Modal analysis (vol%)	
SiO_2	60.77	Or	30.10	alkali-feldspar	2.5
TiO_2	0.15	Ab	47.97	nepheline	3.3
Al_2O_3	17.12	Ne	6.32	sodalite	8.4
FeO	3.19	Ac	7.04	apatite	0.3
Fe_2O_3	2.02	Di	2.90		
MnO	0.27	Fo	0.14	(Σ phenocrysts	14.5)
MgO	0.14	Fa	1.51		
CaO	0.80	Mt	1.09	clinopyroxene	14.5
Na_2O	8.00	Il	0.29	arfvedsonite	8.8
K_2O	5.10	Ap	0.22	aenigmatite	12.8
P_2O_5	0.03				
L.O.I.	1.81			groundmass	49.4
ZrO_2	0.16				
Total	99.56		97.58		100.00

Note: other trace elements analyzed (ppm): Rb = 203, Sr = 20, Cu = 236, Y = 76, and Nb = 272. Zr/Nb = 4.35. Phonolite NK 30 from the Rumpi Hills, Cameroon (Nkoumbou, 1990).

the local environment of Zr in a Na-, Fe-, and Zr-bearing clinopyroxene and in an arfvedsonite sample from a phonolite of the Rumpi Hills volcanic complex (west Cameroon), both containing 1–2 wt% ZrO_2. XAFS is well suited for this study because, unlike single-crystal X-ray diffraction, it is element-specific, and, when fluorescence X-ray detection is employed, it is sensitive to trace to minor levels of a selected element, even in a compositionally complex mineral like the ones examined here. Analysis of Zr*K* edge X-ray absorption spectra provides average interatomic distances, average numbers of neighbors, and the nature of ligands for the first and second shell of neighbors around Zr (see Calas et al., 1987; Brown et al., 1988).

SAMPLE SELECTION AND CHARACTERIZATION

The volcanic province of the Rumpi Hills in western Cameroon is part of the larger-scale structure called the Cameroon Line (Fitton, 1987; Déruelle et al., 1990). These relatively young alkaline volcanics (1–9 m.y. old), comprising basanites, clinopyroxene-rich basanites, trachytes, and phonolites, can be divided into two series on the basis of stratigraphy (Nkoumbou, 1990). Some of the Rumpi Hills basalts have been dated at <1 m.y. old and are much younger than the rest of the lavas, which may or may not belong to different stratigraphic units. Specimen NK 30, which contains the inosilicates used in the present study, is classified as a peralkaline phonolite on the basis of its chemical composition, CIPW norm, and modal composition (Table 1). This phonolite (as many other rocks of this kind) is characterized by a relatively high Zr content (≈1300 ppm).

The phonolite consists of alkali feldspar, nepheline, sodalite, apatite, and three Zr-enriched inosilicates, clinopyroxene, arfvedsonite, and aenigmatite. At the microscopic scale, there are no identifiable Zr-rich minerals. The amounts of clinopyroxene and aenigmatite are roughly equivalent, whereas arfvedsonite is slightly less abundant (Table 1). The textural relationship of these three phases suggests that they probably crystallized at equilibrium and contemporaneously. Selected electron microprobe analyses and average structural formulae for these three minerals are given in Table 2. The Zr content of the clinopyroxenes typically ranges from 0.13 to 5.55 wt% (mean ZrO_2 content ≈ 1.0 wt%), and the arfvedsonite is relatively enriched in Zr (av. ≈ 1.6 wt% ZrO_2). Compared with aenigmatites from other peralkaline rocks, the Rumpi Hills aenigmatite has a low Zr content (≈2000 ppm).

TABLE 2. Representative electron microprobe analyses of three Zr-bearing minerals from phonolite NK 30

	Clinopyroxene*		Arfvedsonite*,**	Aenigmatite*,**
	1	2		
SiO_2	51.83	51.71	47.24	39.65
TiO_2	0.24	0.14	0.18	3.19
Al_2O_3	0.89	0.43	2.59	1.40
FeO*	26.13	24.48	31.50	42.66
MnO	0.91	0.86	1.51	1.84
MgO	0.03	0.06	0.75	0.30
CaO	1.84	4.21	1.47	0.51
Na_2O	12.15	10.39	7.66	6.73
K_2O			1.68	0.04
Nb_2O_5			0.12	0.70
ZrO_2	1.98	5.55	1.97	0.22
Total	96.00	97.83	96.67	97.24
Si	2.09	2.05	7.66	5.82
Ti	0.01	0.00	0.02	0.35
$^{[6]}Al$	0.12	0.02	0.49	0.24
Fe^{2+}	0.12	0.35	3.72	4.40
Fe^{3+}	0.73	0.46	0.54	1.18
Mn	0.03	0.03	0.21	0.23
Mg	0.00	0.00	0.18	0.07
Ca	0.03	0.18	0.26	0.08
Na	0.92	0.80	2.41	1.91
K			0.35	0.01
Zr	0.03	0.11	0.16	0.02
Nb				0.04

Average formulae: acmitic clinopyroxene (48 point analyses):

$$(Na_{0.90}Ca_{0.10})(Fe^{2+}_{0.15}Fe^{3+}_{0.71}Al_{0.05}Zr_{0.02}Ti_{0.01}Mn_{0.02})Si_{2.05}O_6$$

Arfvedsonitic amphibole (12 point analyses):

$$(K_{0.36}Na_{0.64})(Na_{1.74}Ca_{0.27})(Fe^{2+}_{3.6}Fe^{3+}_{0.53}Al_{0.40}Mg_{0.18}Mn_{0.17}Zr_{0.12})(Si_{7.79}Al_{0.21})O_{22}(OH,F,O)_2$$

Ferro-aenigmatite (eight point analyses):

$$(Na_{1.97}K_{0.03})(Fe^{2+}_{4.03}Fe^{3+}_{0.98}Ti_{0.40}Mn_{0.24}Al_{0.20}Ca_{0.07}Mg_{0.07}Nb_{0.02}Zr_{0.01})(Si_{5.90}Al_{0.10})O_{20}.$$

Note: unit formulae based on four cations and six O atoms for the clinopyroxene; 13 cations and 22 O atoms for arfvedsonite; and 14 cations and 20 O atoms for aenigmatite.

* Individual electron microprobe analysis. Fe_{tot} is reported as Fe^{2+}.

** F was not determined in this particular analysis, but amphiboles in other rocks from this province are usually F-rich (1.5–2 wt%).

EXPERIMENTAL DETAILS

Mineral separation

Approximately 10 g of phonolite NK 30 were crushed to obtain grains close to the average size of the mineral crystals (20–30 μm). Feldspars, nepheline, and sodalite were removed using a Frantz isodynamic separator, whereas clinopyroxene was separated using methylene iodide. The procedure was repeated until the isolated fractions appeared sufficiently pure under the microscope. The relative purity of the clinopyroxene and arfvedsonite fractions (≈100 mg of each sample) was also checked

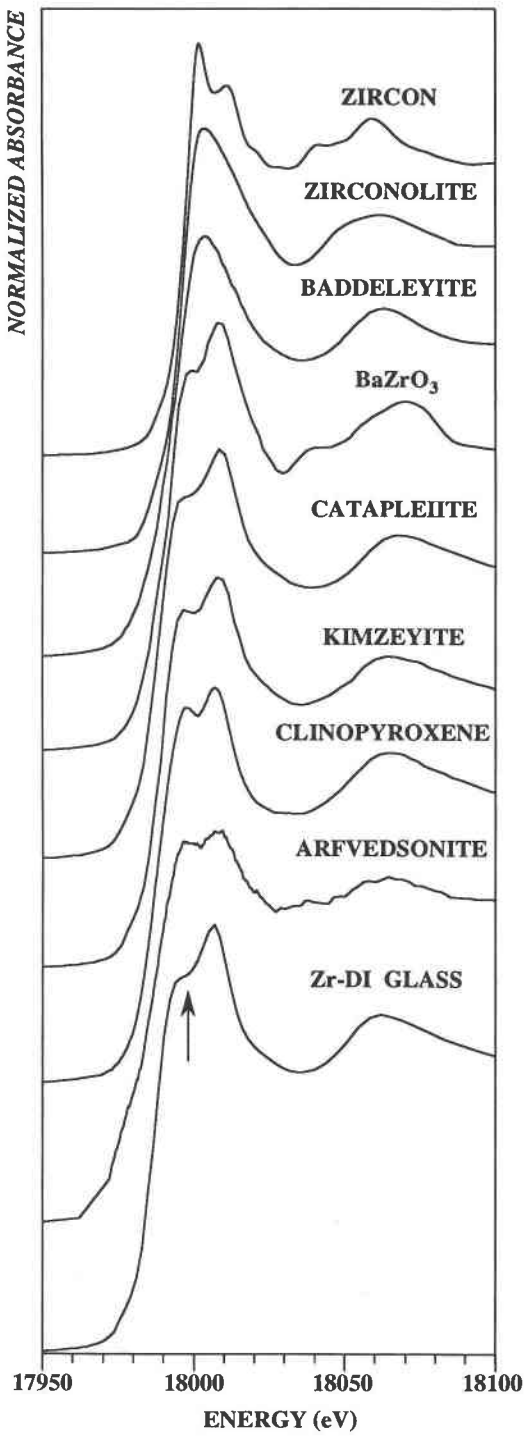

Fig. 1. Normalized XANES spectra of Zr-containing reference compounds (zircon, ZrO_8 site; zirconolite and baddeleyite, ZrO_7 sites; $BaZrO_3$, catapleiite, and kimzeyite, ZrO_6 sites), the two inosilicates studied, and a glass of diopside composition containing 3 wt% Zr (these last data from Farges, 1989). Note the feature on the low-energy side of the $^{[6]}ZrK$ absorption edge, as indicated by the arrow.

using powder X-ray diffraction (Cu$K\alpha$ radiation, operating at 35 kV and 30 mA, calibrated using quartz as an internal standard).

Model compounds for XAFS data collection

A variety of Zr-containing crystalline compounds with well-refined structures were chosen as models of characteristic environments around Zr in minerals and were used to extract XAFS-amplitude and backscattering functions. Nonmetamict zircon from Mud Tanks, Australia (Farges and Calas, 1991), is a model for an $^{[8]}Zr$ environment; $^{[7]}Zr$ occurs in baddeleyite (ZrO_2) and in the $(Ca,REE,Th,U)Zr(Ti,Mg,Fe^{2+})_2O_7$ polymorphs (zirconolite, zirkelite, calciobetafite, and polymignite: Mazzi and Munno, 1983). The baddeleyite used in the present study was a synthetic reagent-grade monoclinic zirconia, 99% pure. We also used a metamict zirconolite from Sri Lanka (sample 111.35 from Ewing et al., 1982, and Farges et al., 1993) that was annealed at 1100 °C for 4 h to induce recrystallization (Mazzi and Munno, 1983; Bayliss et al., 1989). Zr in sixfold coordination is most common in Ca-, Ti-, and Zr-bearing garnets and Zr-bearing alkali silicates. The Zr-bearing garnet used here (containing 30 mol% kimzeyite, $Ca_3(Zr,Ti)_2(Si,Al)_3O_{12}$: Munno et al., 1980) was extracted from an uncompahgrite from Iron Hill, Gunnison County, Colorado (Bahmarane and Velde, 1989 unpublished manuscript). ZrK-edge XAFS analysis for that garnet gives a mean Zr-O distance of 2.07(1) Å, in good agreement with $^{[6]}Zr$-O distances in zirconosilicates and Zr-bearing perovskites. In another kimzeyite crystal from the Stromboli Islands, Munno et al. (1980) suggested that the substitution of Zr by Ti may affect the mean Zr-O distance derived by X-ray diffraction (2.055 Å). The slightly longer mean Zr-O distance derived by XAFS at the ZrK edge confirms this suggestion. Two Na- and Zr-bearing silicates from Mont-Saint-Hilaire, Québec, Canada, were also used as model compounds: catapleiite ($Na_2{}^{[6]}ZrSi_3O_9 \cdot 2H_2O$: Ilyushin et al., 1981) and elpidite ($Na_2{}^{[6]}ZrSi_6O_{15} \cdot 3H_2O$: Cannillo et al., 1973). A previously studied $^{[6]}Zr$-bearing diopsidic glass ($CaO \cdot MgO \cdot 2SiO_2$ + 3 wt% ZrO_2, referred to as Zr-DI) also served as a model compound (Farges, 1989).

Data collection and analysis

All samples were powdered and mounted on Mylar tape. Spectra for reference compounds were collected in transmission mode, whereas XAFS spectra for the two inosilicates were collected in fluorescence mode, with the sample oriented at 45° to the X-ray beam. Data were collected at the Stanford Synchrotron Radiation Laboratory on wiggler beam line IV-1 at the ZrK edge (17998 eV). The storage ring operating conditions were 3 GeV of electron energy and 25–45 mA of electron current, and a Si (220) double-crystal monochromator (energy resolution ≈4 eV at the ZrK edge) was used. At all energies, the monochromator was detuned by 50% to eliminate higher-energy harmonics in the incident X-ray beam. The incident- and transmitted-beam intensities were moni-

tored with an ionization chamber using Ar as the absorbing gas. Because self-absorption is unlikely to be a problem for Zr at these relatively low concentrations, absorbance was measured from the fluorescence yield, and its intensity was monitored with a Stern-Heald type detector (Lytle et al., 1984), with Ar in the fluorescence detector ion chamber. Energy vs. absorbance spectra were obtained by averaging three scans for each sample to improve the signal-to-noise ratio. The data analysis procedure used here is the same as that described in Farges et al. (1991).

Results

Zr X-ray absorption near-edge structure (XANES)

Zr*K*-edge XANES spectra (Fig. 1) for selected Zr model compounds and the two inosilicates show slight but significant differences, depending on the coordination environment of Zr. For [6]Zr-containing compounds, the XANES spectrum is characterized by a shoulder on the low-energy side of the absorption edge. This feature is not observed in XANES spectra of compounds containing [7]Zr (zirconolite and baddeleyite) or [8]Zr (zircon) (Fig. 1). The Zr*K*-edge XANES spectra in the two inosilicates and the [6]Zr reference compounds studied here (catapleiite, $BaZrO_3$, kimzeyite, and Zr-DI glass) are quite similar and indicate the presence of [6]Zr in both minerals. The relatively narrow XANES spectra of the Zr-bearing inosilicates also suggest that the individual Zr-O distances are similar.

Zr X-ray absorption fine structure (XAFS)

Model compounds. Fourier transforms (FT) of the k^3-weighted XAFS spectra at the Zr*K* edge (Fig. 2) for the reference compounds zircon, baddeleyite, catapleiite, and kimzeyite are in good agreement with previous structure refinements (Table 3). The first peak of the FT of zircon corresponds to four O atoms at 2.13 Å and four others at 2.27 Å. The most intense peak corresponds to four Si and four Zr atoms at 3.64 Å, a distance that corresponds to edge-sharing ZrO_8-ZrO_8 and corner-sharing SiO_4-ZrO_8 polyhedra. A weaker contribution from Si second neighbors is at 2.99 Å, corresponding to two edge-sharing SiO_4-ZrO_8 polyhedra. Other longer-range correlations have not been analyzed, although they are readily apparent in the RDF (Fig. 2). These contributions correspond to other ZrO_8-ZrO_8 and SiO_4-ZrO_8 polyhedra, but at greater distance (4.90 Å). In baddeleyite (Smith and Newkirk, 1965), Zr is coordinated by a capped trigonal bipyramid with individual Zr-O distances ranging from 2.02 to 2.43 Å. The ZrO_7 polyhedra share edges, resulting in seven Zr-Zr contributions centered at 3.47 Å. In catapleiite (Ilyushin et al., 1981), the ZrO_6 polyhedra share corners with six SiO_4 tetrahedra and share edges with six NaO_8 polyhedra. This arrangement generates the second major feature in the FT, which corresponds to mean Zr-Si and Zr-Na distances at ≈3.54 and ≈3.71 Å, respectively. Finally, kimzeyite (Munno et al., 1980) is characterized by the presence of ZrO_6 polyhedra sharing edges with CaO_8 polyhedra and AlO_4 tetrahedra.

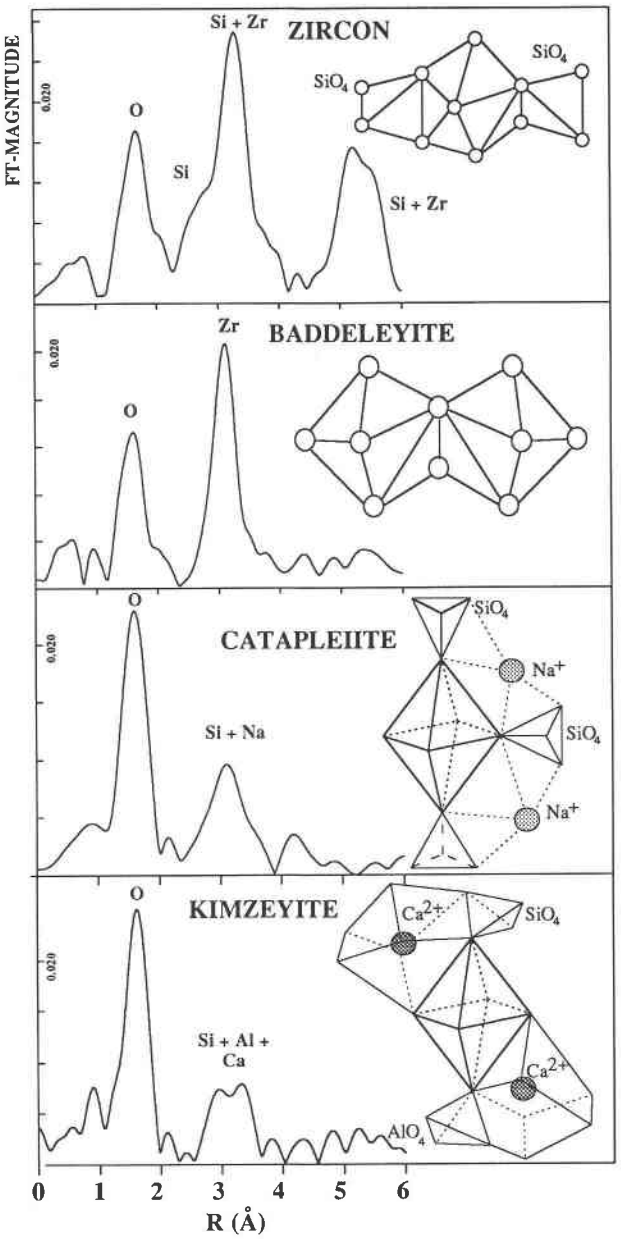

Fig. 2. Fourier transform of the k^3-weighted XAFS spectra for selected minerals: zircon, baddeleyite, catapleiite, and kimzeyite. Peaks in the Zr-X pair correlation functions are labeled to identify X. Peak positions are uncorrected for backscattering phase shift. The calculated corrected interatomic distances are reported in Table 3.

Sodium iron inosilicates. XAFS spectra and FT for clinopyroxene and arfvedsonite are compared with the Zr-DI glass in Figure 3. The first shell of neighbors in each consists of six O atoms. Next-nearest neighbor contributions to the XAFS spectra were best modeled by ≈3(Si + Na) at 3.16 Å and ≈2Fe at ≈3.18 Å from Zr (Table

TABLE 3. Crystalline compounds used for Zr*K*-edge XAFS data reduction

Compound	XAFS results	Structure refinement data	Ref.
	Zr-O*		
Catapleiite	6.0 × O @ 2.07 Å [$\Delta\sigma^2$ = 0.003 Å^2]	6 × O @ 2.073(5) Å	a
Elpidite	6.1 × O @ 2.08 Å [$\Delta\sigma^2$ = 0.003 Å^2]	6 × O @ 2.08(1) Å	b
Kimzeyite	5.8 × O @ 2.07 Å [$\Delta\sigma^2$ = 0.004 Å^2]	6 × O @ 2.05(1) Å	c
Baddeleyite	7.0 × O @ 2.17 Å [$\Delta\sigma^2$ = 0.012 Å^2]	7 × O @ 2.17(8) Å	d
Zirconolite	7.2 × O @ 2.15 Å [$\Delta\sigma^2$ = 0.012 Å^2]	7 × O @ 2.16(8) Å	e
Zircon	7.9 × O @ 2.20 Å [$\Delta\sigma^2$ = 0.010 Å^2]	8 × O @ 2.20(6) Å	f
	Zr-(Si,Na)**		
Catapleiite	12 × {Si + Na} @ 3.64 Å [$\Delta\sigma^2$ = 0.010 Å^2]	6 × Si + 6 × Na @ 3.65(7) Å	a
Elpidite	9.9 × {Si + Na} @ 3.63 Å [$\Delta\sigma^2$ = 0.015 Å^2]	6 × Si + 4 × Na @ 3.6(1) Å	b
Zircon	2.0 × Si @ 2.98 Å [$\Delta\sigma^2$ = 0.006 Å^2]	2 × Si @ 2.990(1) Å	f
	3.7 × Si @ 3.66 Å [$\Delta\sigma^2$ = 0.008 Å^2]	4 × Si @ 3.639(1) Å	f

Note: XAFS-derived Debye-Waller type factors ($\Delta\sigma^2$) are in square brackets; the standard deviation for interatomic distances in crystalline samples is in parentheses (±).

References and sample origin: (a) Ilyushin et al. (1981). Sample from Mont-Saint-Hilaire, Québec (Sorbonne collection, Laboratoire de Minéralogie-Cristallographie, Universités Paris 6 et 7, Paris). (b) Cannillo et al. (1973). Sample from Mont-Saint-Hilaire, Québec (Sorbonne Collection, Paris). (c) Munno et al. (1980). Sample from Iron Hill, Colorado ($[Ca_3Fe_2Si_3O_{12}]_{0.45}[Ca_3Zr_2(Si_2Al)O_{12}]_{0.30}[Ca_3Ti_2(Si_2Al)O_{12}]_{0.25}$: Bahmarane and Velde, 1989 unpublished manuscript). (d) Smith and Newkirk (1965). Sample is 99.5% pure synthetic monoclinic zirconia. (e) Mazzi and Munno (1983). Sample (no. 111.35) from Walaweduwa, Sri Lanka (Museum National d'Histoire Naturelle, Paris), annealed at 1100 °C for 4 h. (f) Hazen and Finger (1979). Sample is 99% pure, synthetic, and nonmetamict $ZrSiO_4$.

* Empirical amplitude and phase shift from $BaZrO_3$: 6 × O @ 2.095 Å (Foëx et al., 1967).

** Theoretical phase shift and amplitude functions (McKale et al., 1988).

4). Attempts to fit the third-neighbor contribution with Zr atoms were unsuccessful. Figure 4a shows the least-squares fit for the clinopyroxene using the curved-wave model (Rehr et al., 1986).

Unfortunately, the little amounts of arfvedsonite recovered from the NK 30 phonolite resulted in an incomplete analysis of the XAFS spectrum because of the low signal-to-noise ratio. Thus only the first atomic shell around Zr could be analyzed (with an accuracy of ±0.04 Å in distance and ±2 atoms in coordination number). However, there is some indication of second neighbors around Zr in that sample (see arrows on the XAFS spectrum in Fig. 3), although no structural parameters could be derived without major constraints in the fit. Figure 4b shows the fit obtained for the first-shell O contribution in arfvedsonite.

Table 4 reports the XAFS-derived parameters from the two inosilicates. The extracted edge-energy (E_0) values for the two inosilicates (17989 and 17990 eV, respectively, for clinopyroxene and arfvedsonite) are in good agreement with those measured in $BaZrO_3$ (17992 eV) within the overall energy resolution (±4 eV). The low absolute value for ΔE_0 ($|\Delta E_0| < 1$ eV) suggests that the empirical amplitude and phase-shift functions extracted from $BaZrO_3$ should provide a good calibration of the XAFS structural parameters.

O neighbors. Inverse Fourier transforms and least-squares fits of the O first-neighbor contribution to the Zr XAFS of the Rumpi Hills clinopyroxene show that the first peak in the FT corresponds to Zr-O correlations at a distance of 2.07(1) Å. This result is in excellent agreement with the measured number of O first neighbors (n = 5.8(5) atoms] and previous XANES results. The mean Zr-O distance measured in arfvedsonite [2.04(4) Å] also is consistent with $^{[6]}$Zr, in spite of the low number of O first neighbors observed (4.5 atoms). This low coordination number is due to the lower signal-to-noise ratio data relative to data collected for the clinopyroxene.

Second neighbors. Fits of the second- and third-shell contributions of the clinopyroxene RDF give mean Zr-(Na,Si) and Zr-(Fe) distances of 3.16(5) and 3.18(5) Å, respectively (Table 4). For both shells, the mean XAFS-derived number of neighbors are 3(1) and 2(1) atoms, respectively. The XAFS spectrum of arfvedsonite also shows a second-neighbor contribution, but, because of the low signal-to-noise ratio, it was impossible to analyze quantitatively. However, qualitative analysis of the inverse FT for this RDF feature suggests the presence of

TABLE 4. Zr*K*-edge XAFS-derived parameters for the clinopyroxene and the arfvedsonite of the NK30 phonolite, compared with a quenched silicate glass

Atomic shells		O*			(Mg Na Si)**			Fe**			Fit quality	
Sample	E_0 (eV)	N	R (Å)	$\Delta\sigma^2$ (Å^2)	N	R (Å)	σ^2 (Å^2)	N	R (Å)	σ^2 (Å^2)	ΔE_0 (eV)	sd†
CPX	17989	5.8	2.07	0.005	3.0	3.16	0.005	1.6	3.18	0.005	−0.3	0.014
ARF‡	17990	4.5	2.04	0.006		—			—		−0.8	0.001
Zr-DI	17991	6.0	2.08	0.007	2.6	3.67	0.005		—		−0.6	0.002

* Using amplitude and phase-shift function from $BaZrO_3$ (Foëx et al., 1967).

** Using theoretical amplitude and phase-shift functions of Si (McKale et al., 1988).

† Standard deviation from the least-squares fit to the data.

‡ Spectra with higher signal-to-noise ratio: the fit was realized on the first contribution of O only.

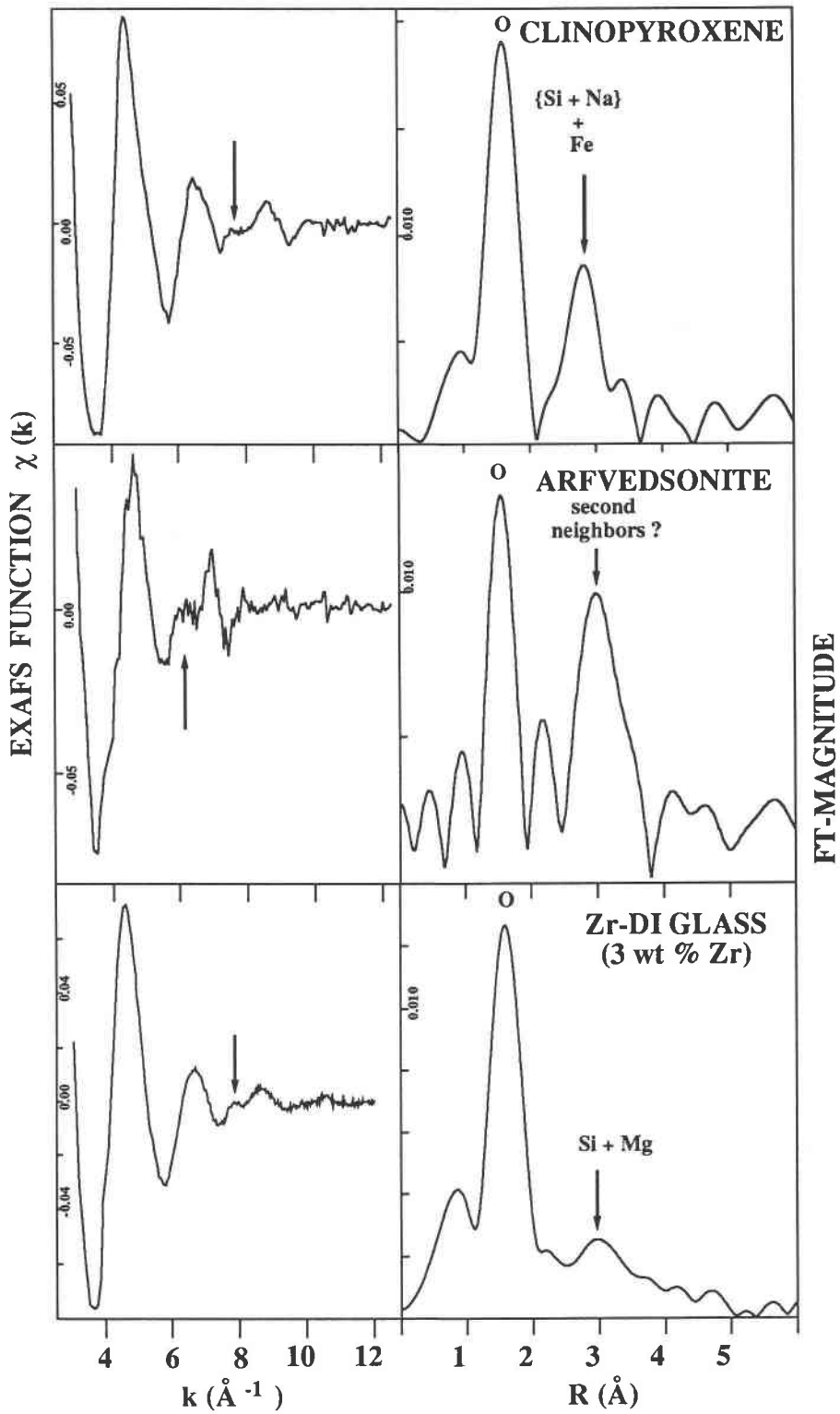

Fig. 3. Fourier transform of the k^3-weighted XAFS spectra for clinopyroxene, arfvedsonite, and a 3-wt% Zr-bearing diopside glass. Peaks in the Zr-X pair correlation functions are labeled to identify X. Peak positions are uncorrected for backscattering phase shift (see corrected interatomic distances in Table 3).

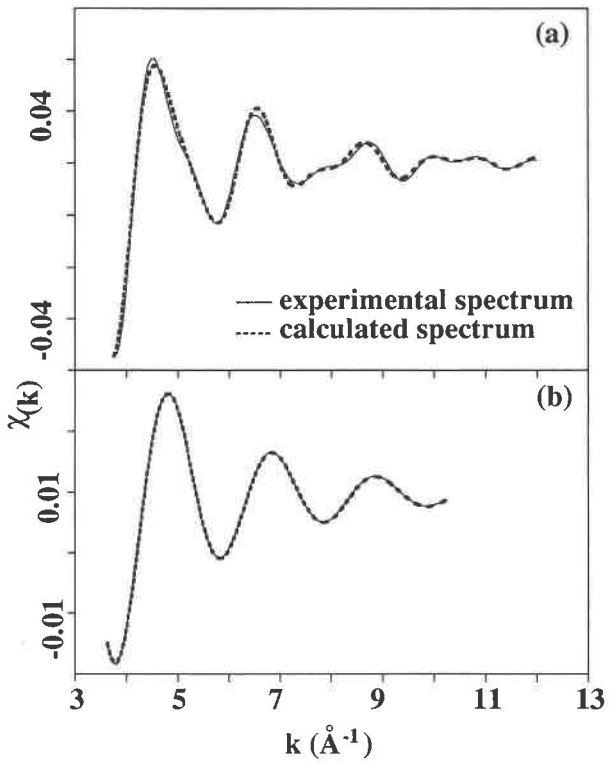

Fig. 4. Least-squares fit of the Fourier-filtered XAFS spectrum of (a) clinopyroxene and (b) arfvedsonite at the Zr*K* edge. The fit for the Zr-bearing clinopyroxene includes contributions from O nearest neighbors and (Si + Na) and Fe second neighbors. The fit for arfvedsonite includes only contributions from O nearest neighbors because of the poor signal-to-noise ratio. The experimental Fourier-filtered XAFS spectrum is shown as a solid curve, and the calculated spectrum is shown as a dashed curve.

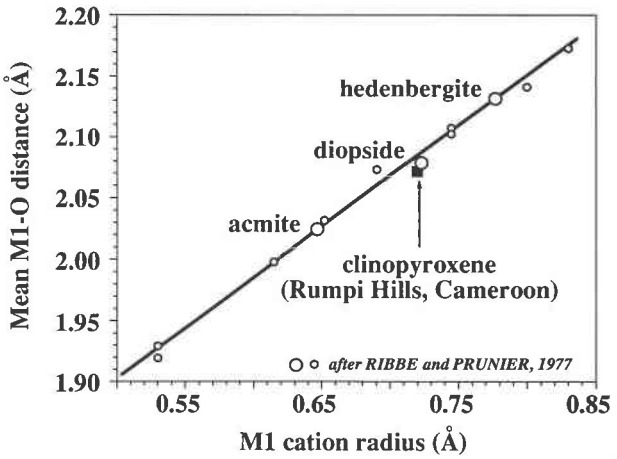

Fig. 5. Ribbe-Prunier correlation (see also Cameron and Papike, 1980) of the mean M1-O distance with a radius of M1 cations for ordered *C*2/*c* pyroxenes. The Zr-, Na-, and Fe-bearing clinopyroxene agrees well with the correlation.

(Si,Na) and possibly Fe second neighbors, as is the case for clinopyroxene. No significant Zr-Zr correlations were observed, indicating no short-range ordering of Zr.

Discussion

Our XANES and XAFS results confirm that Zr is located in sixfold-coordinated sites in the Na- and Fe^{2+}-bearing clinopyroxene and arfvedsonite from Rumpi Hills phonolite NK 30. Significant differences in the XANES, FT spectra, and XAFS-derived structural parameters for Zr model compounds (zircon, baddeleyite, zirconolite, catapleiite, and kimzeyite) and the two Zr-bearing inosilicates rule out the presence of these common Zr minerals as inclusions within the two inosilicates. The presence of sodium iron zirconium silicate inclusions within these inosilicate structures is also excluded because ZrO_6 polyhedra share corners with SiO_4 and FeO_8 polyhedra in these structures. This polyhedral arrangement results in significantly higher mean Zr-(Si,Na) and Zr-Fe distances (≈3.5–3.7 and 4.3–4.5 Å, respectively: Guiseppetti et al., 1971) than those observed in Zr-bearing clinopyroxenes. We have also examined Zr using XAFS methods in other Fe- and Zr-bearing zirconosilicates like tranquilliyite $[Fe_8Ti_3(Zr,Y)_2Si_3O_{24}]$, osumilite- or cupsidine-type structures such as sogdianite $[(K,Na)_2Li_3FeZrSi_{12}O_{30}]$, wöhlerite $[Na_2Ca_4Zr(Nb,Ti)(Si_2O_7)(O,F)_4]$, janhaugite $[Na_3Mn_3(Ti,Zr,Nb)_2O_2(Si_2O_7)_2(OH,F)_2]$, or låvenite $[Na_2(Mn,Ca,Fe)(Zr,Nb)(Si_2O_7)(O,F)_4]$ and found similar results for second-neighbor Zr-Fe correlations.

Zr in the *C*2/*c* clinopyroxene structure

XAFS-derived Zr-O distances in the Rumpi Hills clinopyroxene are in good agreement with the linear correlation (Fig. 5) between the effective ionic radius of M1 cations and the mean M1-O distance for most *C*2/*c* clinopyroxenes (Ribbe and Prunier, 1977; Cameron and Papike, 1980). Hence, Zr should occupy the M1 site in *C*2/*c* clinopyroxene, which is the only sixfold-coordinated site available in these structures (Cameron et al., 1973; Hawthorne, 1976).

We would like to use our XAFS results to constrain possible second-neighbor cation arrangements around Zr in the M1 site of *C*2/*c* clinopyroxene, as knowledge of the medium-range structure around Zr will contribute to our understanding of the geochemical behavior of Zr. Possible second-neighbor cation arrangements around Zr include those present in end-member pyroxenes like acmite, hedenbergite, and diopside, as well as more exotic pyroxene components like $\square ZrSi_2O_6$, $NaZr_{0.75}\square_{0.25}Si_2O_6$, $Na(Fe^{2+}_{0.5}Zr_{0.5})Si_2O_6$, and $CaZrAl_2O_6$ (Jones and Peckett, 1980; McCallum and Charette, 1978), where □ represents a vacancy.

Zr-Fe correlations at ≈3.2 Å in the RDF of the Rumpi Hills clinopyroxene are inconsistent with the presence of significant vacancies around [6]Zr. Furthermore, the lack of observed Zr-Zr correlations rules out local clustering of Zr. Assessment of possible second-neighbor arrangements around Zr cannot be based solely on our XAFS

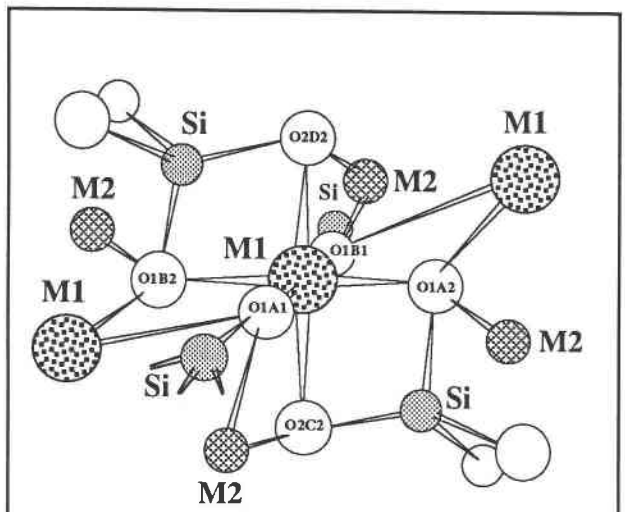

	ACMITE	DIOPSIDE	HEDENBERGITE
(a)	Fe^{3+}	Mg	Fe^{2+}
O1	2.05	2.00	1.90
O2	1.90	1.90	1.85
(b)	$Zr + Fe^{3+}$	Zr + Mg	$Zr + Fe^{2+}$
O1	2.25	2.30	2.35
O2	2.00	2.05	2.15

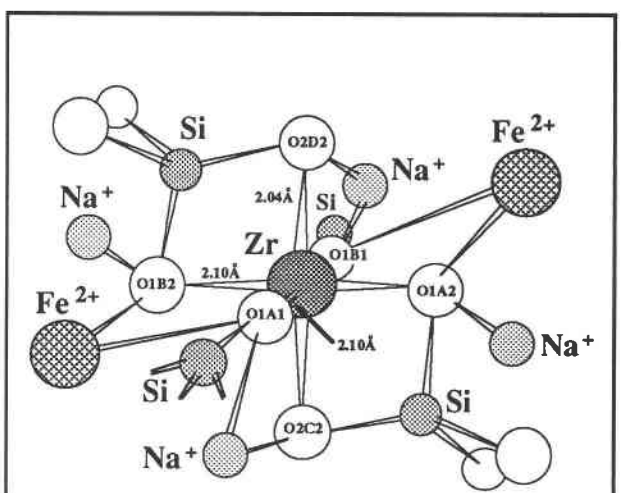

" Na $(Fe^{2+}_{0.5} Zr_{0.5})Si_2O_6$"

(c)	O1		O2	
	d	v	*d*	v
Zr-O	2.10 Å	0.65 v.u.	2.02 Å	0.72 v.u.
Fe^{2+}-O	2.15 Å	0.30 v.u.		
Si-O	1.62 Å	1.00 v.u.	1.59 Å	1.08 v.u.
Na-O	2.40 Å	0.20 v.u.	2.40 Å	0.20 v.u.
	$\Sigma(v)$ =	2.15 v.u.	$\Sigma(v)$ =	2.00 v.u.

Fig. 6. Bond length–bond valence models for M1 sites in a *C2/c* clinopyroxene structure. The O nomenclature is consistent with that of Cameron et al. (1973) and others. The sum of bond valences (v) at O1 and O2 is shown for each M1-site occupancy: (**a**) usual occupancy: all O atoms are reasonably well satisfied; (**b**) Zr occupancy in M1: all O atoms show excess bond valence except O2 in acmite; (**c**) possible environment around ZrO_6 corresponding to the $Na(Fe^{2+}_{0.5}Zr_{0.5})Si_2O_6$ component, satisfying the Zr*K* XAFS results of this study and the valence sum (Brown, 1981). The introduction of Zr in the M1 site makes O1 atoms slightly overbonded. The arrangement may be slightly optimized by a slight radial distortion of the ZrO_6 polyhedra. (Zr-O distances are between 2.02 and 2.10 Å, but the average Zr-O distance remains at 2.07 Å, together with a significant static Debye-Waller type factor for the Zr-O correlation, consistent with XAFS data on site radial distortion: $\Delta\sigma^2_{Zr\text{-}O} \approx 0.005 \pm 0.001$ Å^2.)

results but requires bond valence constraints (see Farges et al., 1991). Possible models of the Zr medium-range environment in the *C2/c* clinopyroxene structure are presented in Figure 6. Substitution of minor quantities of Zr in the M1 site, with adjacent M1(M2) sites containing Fe^{3+}(Na), Mg^{2+}(Ca), or Fe^{2+}(Ca), results in bond valence sums as high as 2.3 vu at the O1 atom (Fig. 6b). Thus this type of substitution appears unlikely. Lengthening of the $(Fe,Mg)^{2+}$-O and Si-O bonds to their maximum observed values in silicates around Zr (2.20 and 1.70Å, respectively: Farges et al., 1991), together with a 0.05-Å radial distortion of the ZrO_6 polyhedra, does not satisfy valence balance.

The presence of $^{[8]}Na^+$ and $^{[6]}Fe^{2+}$ second neighbors around $^{[6]}Zr$ [as in the $Na(Fe^{2+}_{0.5}Zr_{0.5})Si_2O_6$ component] results in bond valence sums of 2.15 and 2.0 vu at the O1 and O2 atoms, respectively (Fig. 6c). The $Na(Fe^{2+}_{0.5}Zr_{0.5})$-$Si_2O_6$ component (or FM-NAZ according to Morimoto et al., 1988) is consistent with our spectroscopic results and bond strength considerations.

The XAFS-derived Zr-O distance for arfvedsonite [2.04(4) Å] is consistent with the three octahedral sites known in this structure (M1, M2, and M3, with M-O distances of 2.115, 2.066, and 2.126 Å, respectively: Hawthorne, 1976). As for clinopyroxene, the XANES spectra for arfvedsonite are significantly different compared with those for alkali zirconosilicates (e.g., catapleiite: Fig. 1; see also Farges, 1989). This excludes the presence of these minerals as inclusions within these inosilicates. In contrast, the similarities of XANES spectra between arfvedsonite and clinopyroxene may suggest that Zr is substituted within this amphibole structure (i.e., with Fe second neighbors around Zr).

Geochemical implications

The peralkaline effect. Zr is expected to have a higher solubility in peralkaline melt compositions than in peraluminous ones (Watson, 1979; Watson and Harrison, 1983) and is dominantly sixfold coordinated by O in similar glasses (Farges, 1989; Farges et al., 1991). In addition,

Zr behaves as a network modifier (Linthout, 1984; Ryerson, 1985) because of a concomitant increase in the proportion of nonbridging O atoms (NBO) to which $^{[6]}$Zr preferentially bonds in the melt (Farges et al., 1991). Because of their strong network-modifying role, the introduction of alkali elements increases the proportion of NBO atoms necessary to accommodate $^{[6]}$Zr, thus inhibiting the formation of $^{[7]}$Zr or $^{[8]}$Zr. The lack of such Zr sites in the melt could conceivably inhibit the crystallization of baddeleyite or zircon, as suggested by Farges et al. (1991), which provides a mechanistic explanation for the incompatible behavior of Zr in peralkaline rocks. In contrast, Zr behaves compatibly in the Rumpi Hills rocks, in part because the inosilicate structures crystallizing from these melts provide sixfold-coordinated sites similar to those occupied by Zr in the melt, as well as a medium-range structural environment that leads to local bond valence satisfaction (Fig. 6c). These factors favor an increase in the crystal-melt partition coefficient of Zr for Na- and Fe^{2+}-rich clinopyroxenes. Similar reasoning may help to explain the observed presence of both $^{[6]}$Zr and $^{[6]}Ti^{4+}$ in other relatively Zr-rich minerals such as kimzeyite garnet (up to 20 wt% Zr: Munno et al., 1980) and ilmenite-ilmenorutile (Zr: 2000 ppm to 4 wt%: Wagner et al., 1988; Pearce, 1990).

Role of f_{O_2}. The oxidation state of the melt may play an indirect role in the partitioning behavior of Zr in peralkaline melts. The low f_{O_2} required to stabilize divalent Fe in peralkaline melts ($f_{O_2} \approx 10^{-11}$ atm: Jones and Peckett, 1980) may explain why Zr-rich clinopyroxenes do not occur in most alkaline series where increasing differentiation is likely to increase the Fe^{3+}-Fe_{tot} ratio in melts. Such an increase should favor the crystallization of Fe^{3+}-rich clinopyroxene, which is an unlikely host for Zr because Fe^{3+} in M1 sites adjacent to Zr would result in an excess of bond valence at O1 atoms around Zr. In addition to this effect, the incompatible behavior of Zr is also favored under oxidizing conditions by the presence of charge-balanced $^{[6]}$Zr-O-(Si,Na) linkages within the melt (Farges et al., 1991). Only low-temperature minerals like Na- and Zr-bearing silicates (e.g., catapleiite) are likely to crystallize from melts at higher f_{O_2} because the local structure around Zr in such minerals is similar to the local Zr environment in the melt. Thus Zr could become compatible late in the crystallization sequence. This sequence of Zr mineral crystallization, involving alternating stages of Zr compatibility and incompatibility, has been observed in differentiated alkaline igneous rocks such as the nepheline syenites and peralkaline granites from Nasarsuk and Motzfelt, Greenland (Jones and Peckett, 1980), where Na- and Fe-rich clinopyroxenes crystallize before alkali-zirconosilicates.

Zr partitioning into other pyroxenes. The crystal-melt partitioning of Zr into clinopyroxenes should be limited by the presence of divalent alkaline-earth cations in the M2 site. Indeed, because of its higher charge compared with alkali elements, Ca would lead to an excess of bond valence at the O1 and O2 atoms around Zr in the M1 sites. This may explain the moderate crystal-liquid distribution coefficients of Zr for diopside ($D^{Zr}_{diopside\text{-}liquid} \approx 0.3$–0.46: Watson and Ryerson, 1986; Lemarchand et al., 1987) compared with Na-, Fe-, and Zr-bearing pyroxenes ($D^{Zr}_{pyroxene\text{-}liquid} > 1$) and their small increase with magmatic differentiation (Ryerson and Hess, 1978; Watson, 1979; Sisson, 1991). In contrast, rock-forming silicates such as olivines or orthopyroxene, with significant amounts of Mg or Fe^{2+} in their M2 sites, cannot effectively partition $^{[6]}$Zr from a melt because this would lead to an excess of bond valence at the associated O atoms.

Acknowledgments

The authors are indebted to the French Ministère des Affaires Etrangères (Programme Lavoisier) for financial support. We thank C. Nkoumbou (Laboratoire de Pétrologie Minéralogique, Université Paris 6) for allowing us to use specimen NK 30 from the Rumpi Hills, Cameroon, P. Bariand (Laboratoire de Minéralogie-Cristallographie, Université Paris 6) and R.C. Ewing (Department of Geology, University of New Mexico at Albuquerque) for providing mineral samples, and W. Jackson, P. O'Day, and B. Hedman (Stanford University) for their assistance with data collection. Reviews from David M. Sherman, E.B. Watson, and Frank C. Hawthorne greatly improved the manuscript. This work was supported by NSF grant EAR-8917437 (G.E.B.). The Stanford Synchrotron Radiation Laboratory is supported by DOE, Office of Basic Energy Sciences, and NIH, Biotechnology Resource Program, Division of Research Resources. IPGP contribution no. 1232.

References cited

Allègre, C.J., Treuil, M., Minster, J.-F., Minster, J.-L., and Albarede, F. (1977) Systematic use of trace elements in igneous processes. I. Fractional crystallization processes in volcanic suites. Contributions to Mineralogy and Petrology, 60, 57–65.

Bayliss, P., Mazzi, F., Munno, R., and White, T.J. (1989) Mineral nomenclature: Zirconolite. Mineralogical Magazine, 53, 565–569.

Brown, G.E., Jr., Calas, G., Waychunas, G.A., and Petiau, J. (1988) X-ray absorption spectroscopy: Applications in mineralogy and geochemistry. In Mineralogical Society of America Reviews in Mineralogy, 18, 431–512.

Brown, I.D. (1981) The bond valence method: An empirical approach to chemical structure and bonding. In M. O'Keeffe and A. Navrotsky, Eds., Structure and bonding in crystals, vol. II, p. 1–30. Academic, New York.

Calas, G., Brown, G.E., Jr., Waychunas, G.A., and Petiau, J. (1987) X-ray absorption spectroscopic studies of silicate glasses and minerals. Physics and Chemistry of Minerals, 15, 19–20.

Cameron, M., and Papike, J.J. (1980) Crystal chemistry of silicate pyroxenes. In Mineralogical Society of America Reviews in Mineralogy, 7, 5–92.

Cameron, M., Sueno, S., Prewitt, C.T., and Papike, J.J. (1973) High temperature crystal chemistry of aegyrite, diopside, hedenbergite, jadeite, spodumene, and ureyite. American Mineralogist, 58, 594–618.

Cannillo, E., Rossi, G., and Ungareti, L. (1973) The crystal structure of elpidite. American Mineralogist, 58, 106–109.

Déruelle, B., Moreau, C., Nkoumbou, C., Kambou, R., Lissom, J., Njonfang, E., Ghogomu, R.T., and Nono, A. (1990) The Cameroon Line: A review. In A.B. Kampunzu and R.T. Lubala, Eds., Phanerozoïc magmatism and structural evolution of African plate, 637 p. Blackie, London.

Duggan, M.B. (1988) Zirconium-rich sodic pyroxenes in felsic volcanics from the Warrumbungle Volcano, Central New South Wales, Australia. Mineralogical Magazine, 52, 491–496.

Dunn, T., and McCallum, I.S. (1982) The partitioning of Zr and Nb between diopside and melts in the system diopside-albite-anorthite. Geochimica et Cosmochimica Acta, 46, 623–629.

Ewing, R.C., Haaker, R.F., Headley, T.J., and Hlava, P.F. (1982) Zirconolites from Sri Lanka, South Africa and Brazil. In S.V. Topp, Ed.,

Scientific basis for nuclear waste management, vol. 6, p. 249–256. Elsevier North Holland, New York.

Farges, F. (1989) Ordre local autour de Zr, Th et U dans des silicates amorphes: Minéraux métamictes et verres silicatés. Thèse de l'Université Paris 7, Paris, France.

Farges, F., and Calas, G. (1991) Structural analysis of radiation damage in zircon and thorite: An X-ray absorption study. American Mineralogist, 72, 60–73.

Farges, F., Ponader, C.W., and Brown, G.E., Jr. (1991) Structural environments of incompatible elements in silicate glass/melts systems. I. Zr at trace levels. Geochimica et Cosmochimica Acta, 55, 1563–1574.

Farges, F., Ewing, R.C., and Brown, G.E., Jr. (1993) The structure of metamict, aperiodic $(Ca,Th)_2Zr_2Ti_2O_{14}$. Journal of Material Research, 8, 1983–1995.

Fitton, J.G. (1987) The Cameroon Line, West Africa: A comparison between oceanic and continental alkaline volcanism. In J.G. Fitton and B.G. Upton, Eds., Alkaline igneous rocks, vol. 30, p. 273–291. Geological Society Special Publications, Washington, DC.

Foëx, M., Traverse, J.P., and Coutures, J. (1967) Etude de la structure cristalline des zirconates alcalinoterreux à haute température. Comptes Rendus de l'Académie des Sciences de Paris C, 264, 1837–1843.

Fujimaki, H., Tatsumoto, M., and Aoki, K. (1984) Partition coefficient of Hf, Zr and REE between phenocrysts and groundmasses (proceedings of the 14th Lunar and Planetary Science Conference, part 2). Journal of Geophysical Research B, 89, 662–672.

Green, T.H., Sie, S.H., Ryan, C.G., and Cousens, D.R. (1989) Proton microprobe-determined partitioning of Nb, Ta, Zr and Y between garnet, clinopyroxene and basaltic magmas at high pressures and temperatures. Chemical Geology, 76, 201–216.

Guiseppetti, G., Mazzi, F., and Tadini, C. (1971) Crystal structure of eudialyte. Tschermaks mineralogische und petrologische Mitteilungen, 16, 105–131.

Hawthorne, F.C. (1976) The crystal chemistry of the amphiboles. V. The structure and chemistry of arfvedsonite. Canadian Mineralogist, 14, 346–356.

Hazen, R.M., and Finger, L.W. (1979) Crystal structure and compressibility of zircon at high pressure. American Mineralogist, 64, 157–161.

Henderson, P. (1982) Inorganic geochemistry, 353 p. Pergamon, Oxford, U.K.

Hildreth, W. (1979) The Bishop Tuff: Evidence for the origin of compositional zonation in silicic magma chambers. Geological Society of America Special Paper, 180, 43–75.

Hofmann, A.W. (1988) Chemical differentiation of the Earth: The relationship between mantle, continental crust, and the oceanic crust. Earth and Planetary Science Letters, 90, 297–314.

Ilyushin, G.D., Voronkov, A.A., Ilyushin, V.V., Nevskii, N.N., and Belov, N.V. (1981) Crystal structure of natural monoclinic catapleiite $Na_2ZrSi_3O_9 \cdot 2H_2O$. Soviet Physics—Crystallography, 26, 808–810.

Jones, A.P., and Peckett, A. (1980) Zirconium bearing aegyrine from Motzfeldt, South Greenland. Contributions to Mineralogy and Petrology, 75, 251–255.

Larsen, L.M. (1979) Distribution of REE and other trace elements between phenocrysts and peralkaline under-saturated magmas, exemplified by rocks from the Gardar igneous province, south Greenland. Lithos, 12, 303–315.

Lemarchand, F., Calas, G., and Villemant, B. (1987) Trace element distribution coefficients in alkaline series. Geochimica et Cosmochimica Acta, 51, 1071–1081.

Linthout, K. (1984) Alkali-zirconosilicates in peralkaline rocks. Contributions to Mineralogy and Petrology, 86, 155–158.

Lytle, F.W., Greegor, R.B., Sandstrom, D.R., Marques, D.R., Wong, J., Spiro, C.L., Huffman, G.P., and Huggins, F.E. (1984) Measurement of soft x-ray absorption spectra with a fluorescence ion chamber detector. Nuclear Instruments and Methods in Physics Research, 226, 542–548.

Mazzi, F., and Munno, R. (1983) Calciobetafite (new mineral of the pyrochlore group), and related minerals from Campi Flegrei, Italy: Crystal structure of polymignite and zirkelite: Comparison with pyrochlore and zirconolite. American Mineralogist, 68, 262–276.

McCallum, I.S., and Charette, M.P. (1978) Zr and Nb partition coefficients: Implications for the genesis of Mare basalts, KREEP and sea floor basalt. Geochimica et Cosmochimica Acta, 42, 859–869.

McKale, A.G., Veal, B.W., Paulikas, A.P., Chan, S.K., and Knapp, G.S. (1988) Improved ab-initio calculations for amplitude and phase functions for extended x-ray absorption fine structure spectroscopy. Journal of the American Chemical Society, 110, 3763–3768.

Morimoto, N., Fabries, J., Ferguson, A.K., Ginzburg, I.V., Ross, M., Seifert, F.A., and Zussman, J. (1988) Nomenclature of pyroxenes. Bulletin de Minéralogie, 111, 535–550.

Munno, R., Rossi, G., and Tadini, C. (1980) Crystal chemistry of kimzeyite from Stromboli, Aeolian Islands, Italy. American Mineralogist, 65, 188–191.

Nkoumbou, C. (1990) 1. Etude géologique des Monts Rumpi: Un ensemble plutonique et volcanique de la "Ligne du Cameroun." 2. Données pétrologiques sur les népéhélinites du Mont Etinde (Cameroun). Thèse de l'Université de Nancy, Nancy, France.

Pearce, J.A., and Norry, M.J. (1979) Petrogenetic implications of Ti, Zr, Y, and Nb variations in volcanic rocks. Contributions to Mineralogy and Petrology, 69, 33–47.

Pearce, N.J.G. (1989) Zirconium-bearing amphiboles from the Igaliko Dyke Swarm, South Greenland. Mineralogical Magazine, 53, 107–110.

——— (1990) Zirconium and niobium-bearing ilmenites from the Igaliko Dyke Swarm, South Greenland. Mineralogical Magazine, 54, 585–588.

Rehr, J.J., Albers, R.C., Natoli, C.R., and Stern, E.A. (1986) New high-energy approximation for x-ray-absorption near-edge structure. Physical Reviews, B34, 4350–4353.

Ribbe, P.H., and Prunier, A.R., Jr. (1977) Stereochemical systematics of ordered *C2/c* silicate pyroxenes. American Mineralogist, 62, 710–720.

Ryerson, F.J. (1985) Oxide solution mechanisms in silicate melts: Systematic variations in the activity coefficient of SiO_2. Geochimica et Cosmochimica Acta, 49, 637–649.

Ryerson, F.J., and Hess, P.C. (1978) Implications of liquid-liquid distribution coefficients to mineral-liquid partitioning. Geochimica et Cosmochimica Acta, 42, 921–932.

Sisson, T.W. (1991) Pyroxene-high silica rhyolite trace element partition coefficients measured by ion-microprobe. Geochimica et Cosmochimica Acta, 55, 1575–1586.

Smith, D.K., and Newkirk, H.W. (1965) The crystal structure of baddeleyite (monoclinic ZrO_2) and its relations to the polymorphism of ZrO_2. Acta Crystallographica, 18, 983–991.

Treuil, M., Joron, J.-L., Jaffrezic, H., Villemant, B., and Calas, G. (1979) Géochimie des éléments hygromagmatophiles: Coefficients de partage minéraux/liquides et propriétés structurales des ces éléments dans les liquides magmatiques. Bulletin de Minéralogie, 102, 402–409.

Wagner, C., Guille, G., Coquillat, J.-L., and Velde, D. (1988) Zr-rich clinopyroxenes in a comenditic trachyte from Mururoa (French Polynesia). Bulletin de Minéralogie, 111, 523–534.

Watson, E.B. (1979) Zircon saturation in felsic liquids: Experimental results and applications to trace element geochemistry. Contributions to Mineralogy and Petrology, 70, 407–419.

Watson, E.B., and Harrison, T.M. (1983) Zircon saturation revisited: Temperature and composition effects in a variety of crustal magmas types. Earth and Planetary Science Letters, 64, 295–304.

Watson, E.B., and Ryerson, F.J. (1986) Partitioning of zirconium between clinopyroxene and magmatic liquids of intermediate composition. Geochimica et Cosmochimica Acta, 50, 2523–2526.

Manuscript received August 9, 1993
Manuscript accepted April 26, 1994